An on-demand plant-based actuator created using conformable electrodes

Li, Wenlong; Matsuhisa, Naoji; Liu, Zhiyuan; Wang, Ming; Luo, Yifei; Cai, Pingqiang; Chen, Geng; Zhang, Feilong; Li, Chengcheng; Liu, Zhihua; Lv, Zhisheng; Zhang ,Wei; Chen, Xiaodong

2021

Li, W., Matsuhisa, N., Liu, Z., Wang, M., Luo, Y., Cai, P., Chen, G., Zhang, F., Li, C., Liu, Z., Lv, Z., Zhang , W. & Chen, X. (2021). An on-demand plant-based actuator created using conformable electrodes. Nature Electronics, 4(2), 134-142. https://dx.doi.org/10.1038/s41928-020-00530-4

https://hdl.handle.net/10356/147451

https://doi.org/10.1038/s41928-020-00530-4

An on-demand electrical phytoactuator enabled by conformable electrodes

Wenlong Li[1,2], Naoji Matsuhisa[1], Zhiyuan Liu[1], Ming Wang[1], Yifei Luo[1], Pingqiang Cai[1], Geng Chen[1], Feilong Zhang[1], Chengcheng Li[1], Zhihua Liu[1], Zhisheng Lv[1], Wei Zhang[1], Xiaodong Chen[1]*

[1]Innovative Center for Flexible Devices (iFLEX), Max Planck–NTU Joint Lab for Artificial Senses, School of Materials Science and Engineering, Nanyang Technological University, 50 Nanyang Avenue, 639798, Singapore.
[2]NTU Institute for Health Technologies, Interdisciplinary Graduate Program, Nanyang Technological University, 61 Nanyang Drive, 637335, Singapore.

Soft actuators can perform delicate tasks through a more adaptive interface with humans than rigid robots. Traditional polymeric soft actuators rely on energy conversion for actuation, resulting in high power input or sluggish responses. Here, we present a plant-based biohybrid actuator (phytoactuator) that requires no energy conversion, is fast responsive, and accessible by CMOS-based electronics. A plant-conformable electrical interface forms the electrical modulating unit and the plant Venus flytrap forms the actuating unit. Frequency-dependent action potential modulation was discovered to realize fast and accurate plant actuation. The response time of the phytoactuator can be tuned to 1.3 s, with a power input of only 10^{-5} W. Our phytoactuator can be installed on other platforms and controlled wirelessly using smartphones. It can grasp very thin wires or capture moving objects on demand. Such a plant-based device could lead to the development of various plant bioelectronics such as plant robots and plant healthcare devices.

Soft actuators with a high degree of compliance can easily deform to delicate task settings and unstructured environments, realizing more adaptive and comfort interfaces for human-machine and human-environment[1-5]. Materials and structural engineering have enabled various soft actuators by fluidic/pneumatic elastomers[6], shape-memory[7] or electroactive[8] polymers. However, energy conversion is required in such artificial polymeric materials for shape-changing or mechanical movement, leading to high power input or sluggish responses. While biohybrid actuators using contractile muscles[9, 10] or mobile cells[11, 12] require minimal power input, cells or tissues are complicated to prepare and their actuation is relatively unpredictable[13, 14]. In this regard, biohybrid actuators which not only inherit the merits of organismal components, but also possess properties such as high speed, high accuracy, and compatibility with current electronic systems are needed.

Plants, despite being rarely appreciated, possess phenomenal intelligence. For instance, parasitic dodder (*Cuscuta*) can make delicate decisions to coil around the profitable host and take the host's resources for their life[15]. Venus flytrap (*Dionaea muscipula*) can lock insects in its attractive lobes, from which even the agile fly fails to escape[16]. Furthermore, the behavioural plasticity[17], network-like communication[18], ability of learning and memory[19], sophisticated morphogenesis[20, 21], and intricate microstructures[22, 23] all demonstrate impressive intelligence in plants.

Venus flytrap is an intelligent thigmonastic plant, where touches on its upper epidermis generate action potentials (APs) that can trigger rapid flytrap closing[24, 25] (Supplementary Fig. 1 - 3). We exploit the flytrap's thigmonastic response to build on-demand actuator devices. Because flytrap actuation is triggered internally by electrophysiological signals[26], we hypothesized that artificial interference with the plant's electrophysiology through external electricity could, in theory, modulate its actuation behaviour. The ability to electrically modulate the flytrap electrophysiology could potentially realize on-demand actuation and allow the flytrap to be accessed by CMOS (complementary

metal-oxide-semiconductor)-based electronics. Such a possibility will create a whole new area of plant-integrated bioelectronics.

To electrically interfere with the plant's electrophysiology for a bioelectronics application, two key challenges present. The first is the physical interface to communicate with plants. Such an interface should be integrated on the plant surface without affecting plant movement or physiology. Different from human skin, the plant surface is protected by a hydrophobic waxy cuticle layer, making attachment of thin-film electronic devices difficult. The other challenge is the effective electrical information to be communicated with plants. Currently, no formatted electrical communication methods with plants exist. Though the phenomenon of electrostimulation-induced flytrap closure was reported, the mechanism is not clear and accurate modulation has not been achieved.[27, 28]

In this Article, we show a conformable plant electrical interface to modulate the electrophysiology of Venus flytrap plants. Plant-conformable electrodes were developed as a physical interface and frequency-dependent action potential modulation was explored as an electrical communication protocol for plants. Based on these, a plant-based actuator (noted as phytoactuator in this paper) is presented using Venus flytrap lobes as the actuating unit and conformable electrodes as the electrical modulating unit (Fig. 1a). The electrical phytoactuator requires no energy conversion and is power-efficient (input voltage and power as low as 1.5 V and 10^{-5} W, respectively), fast responsive (response time can be modulated to ~ 1.3 s), compatible with CMOS-based electronics (easily accessed by WiFi module for wireless smartphone control), modular and installable to various platforms (can be isolated from plant stem and integrated on a finger, robotic hand, manipulator, etc.), and capable of capturing fine and moving objects.

Conformable electrodes for plant electrical modulation

To modulate the flytrap electrophysiology, plant electrodes that can either detect electrical signals from the plant or deliver an electrical field to the plant are needed[29]. Traditional electrode protocols (Supplementary Fig. 4) adopted by plant biologists include intracellular methods (glass microelectrodes[30] or aphid stylet electrodes[31]) and extracellular methods (inserted wire electrodes[32] or surface Ag/AgCl-Agar electrode[16, 33]). While suited for fundamental studies of plants, these methods cannot be implemented in a bioelectronics device because they are invasive, easily detached from plants, and require complicated setup procedures. While a vapor printing method of a conductive polymer on plant surface was recently reported, the harsh printing condition (slight heating and diluted acid solution washing) makes it unsuitable for most sensitive and fragile plants.[34] Electrodes for the phytoactuator devices should ideally be non-invasive, compliant with the plant morphology and movement, miniaturized and portable, and effective at ionic-electronic current transduction. Achieving this requires the electrode to conform to the surface of the plant (Supplementary Fig. 5). However, this is challenging because the plant epidermis has a waxy cuticle layer containing rough microstructures[23].

Our conformable electrode resolves these issues through a soft and adhesive hydrogel layer as the plant-contacting layer and Au nanomesh on polydimethylsiloxane (PDMS) as the electronic transduction layer (Fig. 1b). The conformable electrode system can simultaneously deliver customized modulating electricity to and detect electrical signals from the plant, offering a way to monitor electrophysiological signals of the plant during electrical modulation (Fig. 1a). The conformable electrode is also non-invasive in that it only senses or induces capacitive currents in plant tissue separated by the cuticle layer, while no electrochemical reaction takes place between the plant and the electrode. The adhesive hydrogel is prepared from the thermo-polymerization of acrylic acid monomers with 10 mM KCl ionic additive[35]. The adhesive poly(acrylic acid) hydrogel film allows the electrode to adhere and conform to the plant surface (Fig. 1c). In a 90º peel-off test from the plant surface,

electrodes with a hydrogel layer recorded an adhesive strength of 15.6 N/m while electrodes without hydrogel showed negligible adhesion (Fig. 1d). This confirms that an adhesive interface between the hydrogel layer and the plant surface exists. The hydrogel layer is also ionically conductive, stretchable, biocompatible, and transparent enough for normal chlorophyll activity to occur (Supplementary Fig. 6 and 7).

For the electronic conduction layer, we synthesized Au nanomesh film using wet chemistry (Supplementary Fig. 8 - 10)[36, 37] and transferred the two-dimensional intertwined Au nanomesh network that formed at the water surface onto PDMS. The Au nanomesh-PDMS film was sufficiently transparent for effective plant light absorption (Supplementary Fig. 11). The film was highly stretchable, stable upon 50% strain cycling, and remained conductive even at 135% strain (Supplementary Fig. 12). The interfacial current transduction between the Au nanomesh and adhesive hydrogel is also highly efficient (Supplementary Fig. 13), as the interfacial admittance of Au nanomesh with adhesive hydrogel is higher than those of carbon nanotube (CNT), silver nanowire (AgNW), and aluminium (Al) film. Also, the conformable electrode is only ~ 4.9 mg, much lighter than a flytrap lobe (~ 228 mg), presenting a negligible weight effect when attached to flytrap (Supplementary Fig. 14 and Supplementary Table 1). These results demonstrate that our conformable electrodes, which are conductive, transparent, lightweight, easy to apply, and conform well to plant surfaces, form a promising biocompatible electrical interface for sensing and modulating plant electrophysiology. It also provides a new avenue for the development of plant bioelectronics based on biocompatible adhesive hydrogels.

Compared to the current gold standard non-invasive Ag/AgCl-Agar electrodes used for plant surface potential measurements[12,13], our conformable electrodes attached better to the flytrap lobe from the open to close state (Fig. 1e). This firm adhesion ensures continuous and accurate sensing of electrical signals and delivery of modulating electricity and is necessary because the flytrap has a fast nastic response. As shown in Fig. 1e, Ag/AgCl-Agar

electrodes detached easily from the leaf epidermis during flytrap closure. On-plant impedance measurements show that the firm adhesion of the conformable electrodes lowers contact impedance (Fig. 1f). Conformable electrodes showed an impedance of ~300 kΩ compared to ~1 MΩ for Ag/AgCl-Agar electrodes at low frequencies (1 – 10 Hz). The lower on-plant impedance of conformable electrodes also agreed well with AP signal measurements. The shape of the AP signals obtained from both the conformable electrodes and Ag/AgCl-Agar electrodes were comparable (Fig. 1g and Supplementary Fig. 15-16). Analysis of nine AP signals (Fig. 1h) further verified that conformable electrodes (92.7 ± 3.7 mV) presented a larger signal amplitude than Ag/AgCl-Agar electrodes (70.6 ± 5.8 mV). These results show that our conformable electrodes are well-suited for electrical interfacing with plants.

Electrical modulation of flytrap

Using the conformable electrodes, we show that each mechanical touch induces one AP and it takes two successive APs to close the flytrap lobes (Supplementary Fig. 17), which agrees with literature[26]. The time interval between the two touches, however, must be no longer than 60 s for the lobes to close; intervals longer than 60 s will not close the lobes (Supplementary Fig. 18). These results confirm that mechanical perception is transduced into an electrophysiological signal in the form of AP and that the flytrap is capable of memory – it can register the first AP and compute two successive APs within 60 s to initiate lobe actuation (Supplementary Fig. 19)[26].

To electrically actuate the flytrap, we attached a pair of conformable electrodes on each of the two lobes (Fig. 2a). One pair of electrodes is for stimulation and the other pair is for acquiring potential signals. Flytrap actuation is measured by a normalized lobe edge distance, y/y_0, where y refers to the edge distance of the two lobes and y_0 is the initial edge distance before flytrap actuation. Upon DC (direct current) 3V stimulation, one AP was generated immediately, followed by a series of APs during a stimulation period of 40 s (Fig.

2b-c). Interestingly, similar to the mechanical stimulation of flytrap shown in Supplementary Fig. 17, electrical stimulation also induces lobe closure after the second AP (Fig. 2c), indicating that two APs are also needed in electrical flytrap actuation. Different DC voltage stimulations from 0.5 V to 3 V show a threshold voltage of around 1.5 V (Fig. 2d and Supplementary Fig. 20). A series of autonomous APs were observed for stimulations ≥ 1.5 V whereas no APs were seen for those stimulated at < 1.5 V (Fig. 2e). Indeed, we found that almost all the electrical actuation cases were linked with the appearance of a second AP. To verify this, the response time (defined as the time interval between the start of stimulation and start of flytrap actuation, extracted from y/y_0 data) and first two-AP interval (defined as the time interval between the first and second AP during DC stimulation, extracted from potential signal data) were compared (Figure 2f). Linear fitting of response time versus the first two-AP interval showed a strong correlation of the two with an R-square of 0.986, indicating the important role of two APs in electrical flytrap actuation. Moreover, simultaneous current density measurements also displayed spikes that coincide with the appearance of APs for stimulating voltages ≥ 1.5 V, demonstrating the increase in plant tissue conductance is related to AP generation (Supplementary Fig. 21). Changing the electrode geometry and position shows no distinguishable differences in flytrap actuation under DC stimulation (Supplementary Fig. 22-23), indicating an isotropic presence of excitable tissues in flytrap.

Though the phenomenon of electrically-induced flytrap closure and a threshold of 1.5 V was reported in the literature, previous studies on electrical stimulation of flytrap used charge-injection capacitor or function generator by invasive silver wire electrodes, and the electrically induced flytrap closure was attributed to direct charge injection into the flytrap motor cells[27, 28]. Our non-invasive conformable electrode system avoided direct charge injection into flytrap tissue but only induce capacitive current flow inside plants. Moreover, simultaneous potential signal and current density measurements confirm the generation of

APs. Our results suggest that flytrap closure by electrical stimulation is similar to mechanical stimulation in that it relies on two-AP memory and computation.

It is further noted that the AP intervals – the time duration between two autonomous APs induced by DC stimulation – are random (Fig. 2e and Supplementary Fig. 24). However, an analysis of 376 AP intervals in DC stimulation showed that a minimum limit of 1.2 s exists (Fig. 2g). Such a limit resembles the refractory period of neurons, where it is defined as the time during which another AP cannot be generated due to the generation of the first AP. The AP interval limit in our experiment suggests that the refractory period of flytrap is likely around 1.2 s, which is much longer than the refractory period of neurons (a few milliseconds). To further verify the AP refractory period in the flytrap, we mechanically stimulated the flytrap twice within 0.3 s and found that it remained open even after two touches, indicating that two APs cannot be generated within the refractory period (Supplementary Fig. 18). In contrast to the previous estimation of the flytrap AP refractory period (3 – 5 s) induced by light[38], our results show direct experimental proof of the flytrap AP refractory period in electrical stimulation. In summary, the two-AP mechanism and the refractory period in flytrap during electrical stimulation provide a biological basis for developing plant communication protocols to realize accurate phytoactuation.

While DC stimulation above 1.5 V can induce a series of APs for flytrap closure, the appearance of second AP, thus the response time for flytrap closure, is usually random (Supplementary Fig. 20). When the electrical stimulus was changed from DC to a square wave, the actuation behaviour could be modulated faster and more accurately (Supplementary Fig. 25). Under a stimulating frequency of 0.1 Hz, the response time generally takes 4.7 ± 1.4 s (Fig. 3a). Increasing the frequency to 0.5 Hz significantly reduced the response time to 1.8 ± 0.4 s. However, beyond 0.5 Hz, the decrease in response time plateaus. At 2 Hz, response time decreased only to 1.3 ± 0.1 s. To understand how stimulating frequency modulates response time, we registered potential signals with two conformable electrode pairs during

square wave stimulation. A square wave contains a rising edge and a falling edge, each of which induced one AP (Fig. 3b). In contrast, a “dead” flytrap showed no rising-edge and falling-edge AP during square wave modulation (Supplementary Fig. 26). As a result, one square wave can accumulate exactly two APs for flytrap actuation, explaining the reason for the frequency-dependent modulation of the response time. However, by converting stimulating frequency (*f*) to the rising-falling edge interval (*t*) using the expression $t = 1/(2f)$, the response time is predicted as 0.25 s at 2 Hz, which significantly deviates from the experiments. Instead of approaching 0 s as the frequency increases, response time approached 1.3 ± 0.1 s. Together with Fig. 2g showing a refractory period of 1.2 s, these results demonstrate that the frequency modulation is limited by the refractory period and therefore, two APs cannot be generated within this period. More importantly, the convergence of response time from random under DC stimulation to refractory period limit under 2 Hz frequency modulation indicates that most flytraps share a similar refractory period. This is the biological basis for accurate modulation of flytraps on different samples. To further explain the AP generation in DC stimulation and frequency-dependent modulation, we propose a qualitative hypothesis that involves the capacitive charging of flytrap excitable membrane using an external electrical field. The detailed discussion can be found in the Supplementary Information (Supplementary Fig. 27).

The fact that plants usually grow in pots makes the practical applications difficult when converting plants into bioelectronic devices. For better device mobility and portability, we explored the modular property of Venus flytrap. The flytrap lobes were isolated from its petiole (the supportive connection to the roots) and the cut was sealed with Ecoflex elastomer to prevent tissue dehydration. Interestingly, the modular flytrap lobes continued to display good electrical actuation for up to one day. For more prolonged survival, better methods to prevent dehydration must be explored. As shown in Fig. 3c and Supplementary Fig. 28, the response time of modular flytrap (16.2 ± 10.4 s) was retarded compared with flytrap in pots

(6.8 ± 5.2 s). However, the 2 Hz square wave modulation can eliminate such retardation, approaching the response time limit of 1.3 s. Also, as shown in Fig. 3d, the 2 Hz square wave modulation can increase the normalized actuating speed (maximum value of $-2.8 \pm 0.4\ s^{-1}$) compared with DC modulation (maximum value of $-2.0 \pm 0.8\ s^{-1}$). These results show that modular flytraps can work well without any actuation performance loss using frequency modulation, providing the possibility to install the phytoactuator, in principle, on any other devices or platforms.

Our electrical phytoactuator with a response time of 1.3 s is faster than most of the recent soft electrical actuators (Supplementary Fig. 29, Supplementary Table 2 and 3). Also, the phytoactuator only requires a voltage input of 1.5 V at a power consumption of 10^{-5} W, which is 4 – 5 orders of magnitude smaller than traditional devices (1 – 0.1 W). The phytoactuator has such a fast response time and low power consumption because actuation is completed by the flytrap itself. Electrical energy serves only as a stimulus and is not converted to mechanical energy for actuation. This feature presents an out-of-the-box strategy for developing actuator devices based on natural resources such as plants; our task is to find ways to interface with and modulate the various intelligent systems found in Nature. However, one issue related to reversibility remains. Though the closure process can be accurately modulated, it takes hours to naturally reopen the flytrap. Electrical modulations showed no effect in accelerating flytrap reopening. As the closing process involves a fast release of hydroelastic energy between the outer and inner layers of flytrap[39], accelerating the re-storage of hydroelastic energy between the two layers may accelerate flytrap reopening.

An on-demand electrical phytoactuator

In light of the increasing dependence on the cyber interface for human-environment interactions, we tested the modular flytraps by implementing a smartphone-controllable phytoactuator (Fig. 4a-b, Supplementary Fig. 30, and Supplementary Movie). Because our

phytoactuator has a low 1.5 V threshold voltage, it is accessible to cyberspace through miniaturized electronic systems (such as a typical WiFi chip with an output voltage of 3.3 V). As shown in Fig. 4a-b, the command by the user in a smartphone application is sent via the Internet to a WiFi module (ESP8266) containing a General Purpose Input Output (GPIO). Upon receiving the command, the WiFi module sends a 3.3 V electrical output to the conformable electrodes, which initiates the actuation of the flytrap lobes. This experiment shows the modular phytoactuator can communicate with CMOS-based electronics via our conformable electrodes on-demand. Compared with the dedicated electrostimulation setups in the literature (such as low noise function generator, optocoupler insolation, and signal conditioning circuits)[27, 28], the cell phone trigger is based on a WiFi chip that is lightweight (~ 10 g), programable, and accessible by the Internet. This presents a possibility of connecting plants into the cyberspace.

While conventional robots are good at performing repetitive tasks in well-structured and well-defined environments, they are less efficient when it comes to handling undefined objects in changing environments. For example, the robotic hand would typically struggle to pick up small and fine objects. In contrast, with the hair-like cilia projections lining the lobe edge, the flytrap is capable of grasping and tightly locking small insects such as mosquitoes. We combined the positioning capabilities of a robotic hand with the grasping abilities of the phytoactuator by attaching the isolated phytoactuator on a robotic hand. After careful positioning of the robotic arm, the flytrap was activated through the smartphone as before, causing the lobes to close and pick up a thin (0.5 mm diameter) platinum wire (Fig. 4c and Supplementary Movie). Because the response time of our phytoactuator can be accurately modulated, we show it can also be used in dynamic environments to capture moving objects (Fig. 4c and Supplementary Movie). If the kinetic information of the moving object is known, the capturing task can be implemented by buffering the response time in advance. For

example, for a 1 g weight of object falling at a speed of 1 cm/s, the phytoactuator mounted on a manipulator can be modulated to capture the object as it falls through the lobes.

Conclusions

In summary, we reported a conformable electrical interface to construct an electrical phytoactuator with the Venus flytrap lobe as the actuating unit and conformable electrodes as the modulating unit. The conformable electrodes were used to modulate the flytrap electrophysiology and perform on-demand actuation of the lobes. We show the phytoactuator can be combined with a robotic arm to pick up a fine wire or modulated independently to capture a moving object. The conformable electrical interface in this work can provide a new toolkit for plant studies and plant bioelectronics development. The ability to interfere with the plant's electrophysiology through external electricity opens new possibilities for building plant communication protocols. More importantly, as shown in our study, plants are modular and can be isolated and installed on a variety of platforms. Integrating with current soft electronics[40-42] or plant-based electronics[43-45], such modularity in plant functionalities can potentially be exploited to build various plant-based robots, sensors, memristors, ionic circuits, and plant healthcare devices in the future.

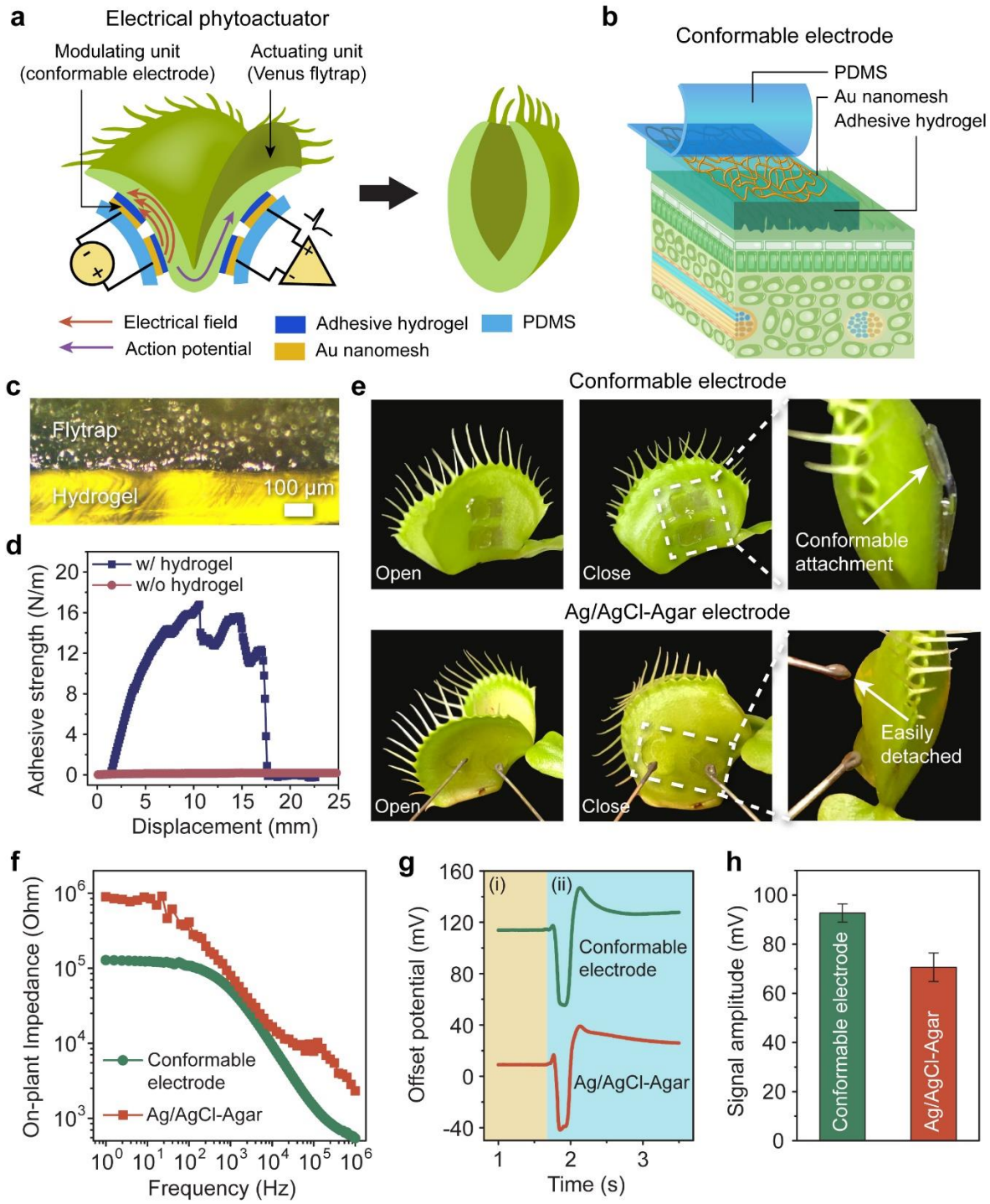

Fig. 1 | Electrically modulated biohybrid phytoactuator. a, Left: Schematic of the phytoactuator. Venus flytrap is the actuating unit and conformable electrodes form the modulating unit. The conformable electrode system can deliver electric field onto the flytrap and simultaneously measure electrical signals, i.e., APs, from the flytrap. Right: Schematic showing a closed flytrap lobe after electrical actuation. b, Schematic of the conformable electrode attached to the surface of a leaf. The plant interface layer is an adhesive hydrogel

while the electronic conduction layer is an Au nanomesh-PDMS layer. c, Optical micrograph of a cross-section of the flytrap and adhesive hydrogel shows the conformable attachment of the hydrogel. d, In a 90° peel-off test, electrodes with a hydrogel layer sustained an adhesive strength of 15.6 N/m while electrodes without hydrogel have negligible adhesiveness. e, Photos of a conformable electrode (top row) and traditional Ag/AgCl-Agar (bottom row) on flytrap epidermis. Conformable electrodes remain attached to the flytrap epidermis in both the open (left) to closed (middle) state. Zoomed-in view (right) shows conformable electrodes conform to the epidermis in the closed state. Ag/AgCl-Agar electrodes (brown rods) attached to the flytrap epidermis in the open state (left) but detached easily in the closed state (middle and right). f, Conformable electrode has a smaller on-plant impedance than Ag/AgCl-Agar electrode. g, Representative AP signals obtained from conformable electrode and Ag/AgCl-Agar electrode. Electrical signals before (i) and after (ii) mechanical touch. h, Signal amplitude analysis of nine AP signals show conformable electrodes give a larger signal amplitude than Ag/AgCl-Agar electrodes. Error bars are s.d. from nine samples.

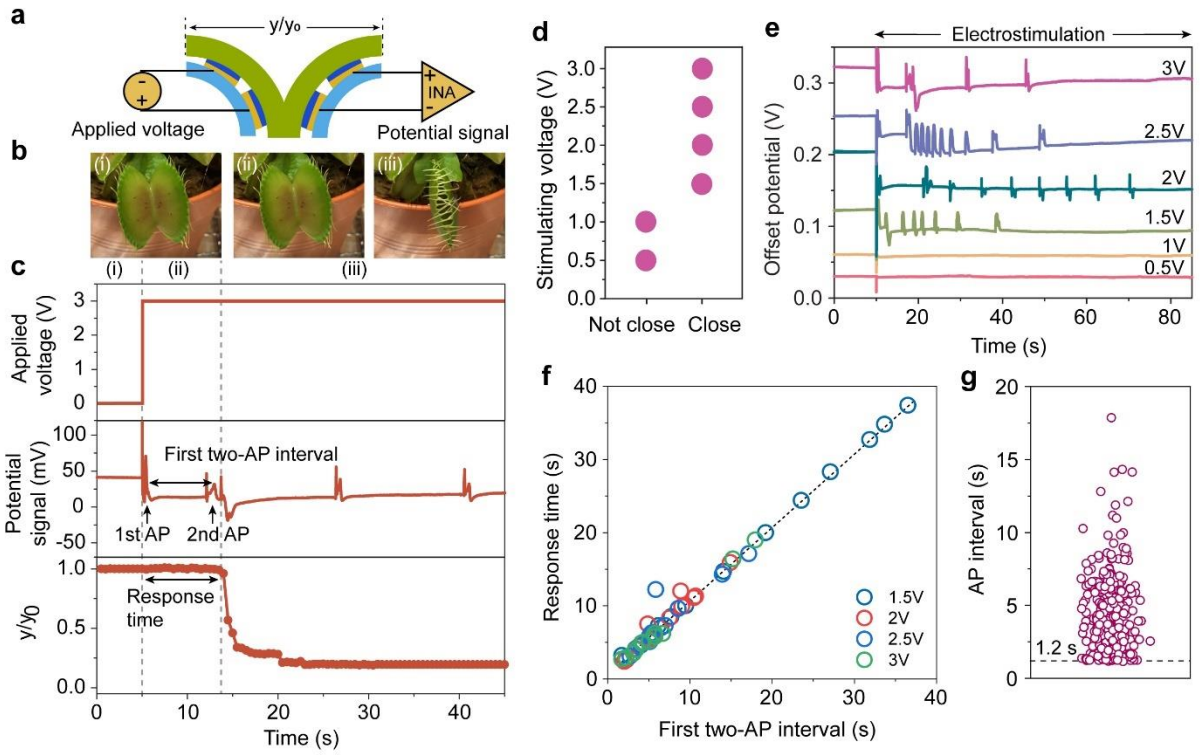

Fig. 2 | DC voltage stimulation of flytrap. a, Schematic showing a pair of conformable electrodes attached to each flytrap lobe. The left lobe is stimulated by the applied voltage (DC 3 V) and potential signals are acquired from the right lobe. Lobe closing is determined by the lobe edge distance, y/y_0, where y is the distance at any time and y_0 is the initial distance before actuation. INA: instrumentation amplifier for data acquisition. b, Photograph snapshots of flytrap stimulated by DC 3 V. c, Simultaneous recording of potential signal and y/y_0 when a DC 3 V is applied. Upon applying voltage, the 1st AP formed immediately, followed by a series of APs. Flytrap closes after the 2nd AP. d, Flytraps stimulated at different voltages show a threshold voltage of 1.5 V for phytoactuation. e, Offset potential signals acquired from conformable electrodes over 75 s at different DC stimulating voltages. f, Correlation of response time and first two-AP interval for different DC stimulations, confirming the two-AP mechanism in electrical stimulation. Each voltage group was repeated with 12 samples. g, AP interval analysis in AP series generated by DC stimulations, indicating the refractory period of around 1.2 s in flytrap. The black dashed line indicates a reference for 1.2 s. The number of AP intervals analyzed: 376.

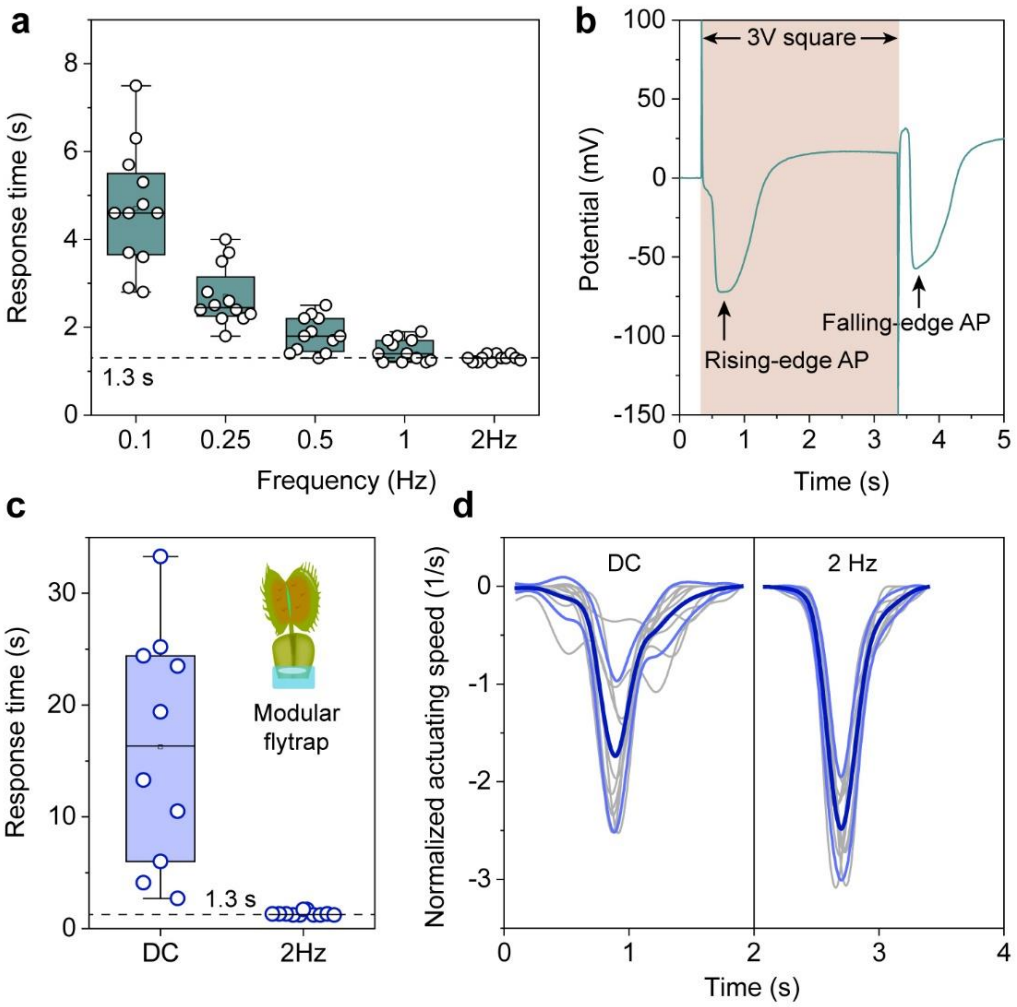

Fig. 3 | Frequency-dependent modulation of flytrap electrophysiology and actuation behavior. a, Modulation of flytrap response time by different frequencies. The black dashed line indicates a reference for 1.3 s. Middle line, median; box, upper and lower quartiles; open square in the box, mean; bar, 1.5 times interquartile range; Open circles represent data points. Each frequency group was repeated by 12 samples. b, Potential signal measurement, when stimulated by a 3 V square wave, shows one AP forms immediately following each rising edge and falling edge of the square wave. c, DC modulation on the modular flytraps shows large response time (16.2 ± 10.4 s) while 2 Hz square wave modulation can approach the response time limit of 1.3 s. The inset shows schematic of the modular flytrap. The black dashed line indicates a reference for 1.3 s. Middle line, median; box, upper and lower quartiles; open square in the box, mean; bar, 1.5 times interquartile range; Open circles

represent data points. Each sample group was repeated by 10 samples. d, Actuating kinetics of modular flytraps show accelerated actuating kinetics by 2 Hz square wave modulation. The normalized actuating speed was obtained by taking the first-order derivative of y/y_0 data in Supplementary Fig. 28. The dark blue line represents the mean and the light blue line represents the s.d. of normalized actuating speeds for 10 samples. The overlapped grey lines represent raw data.

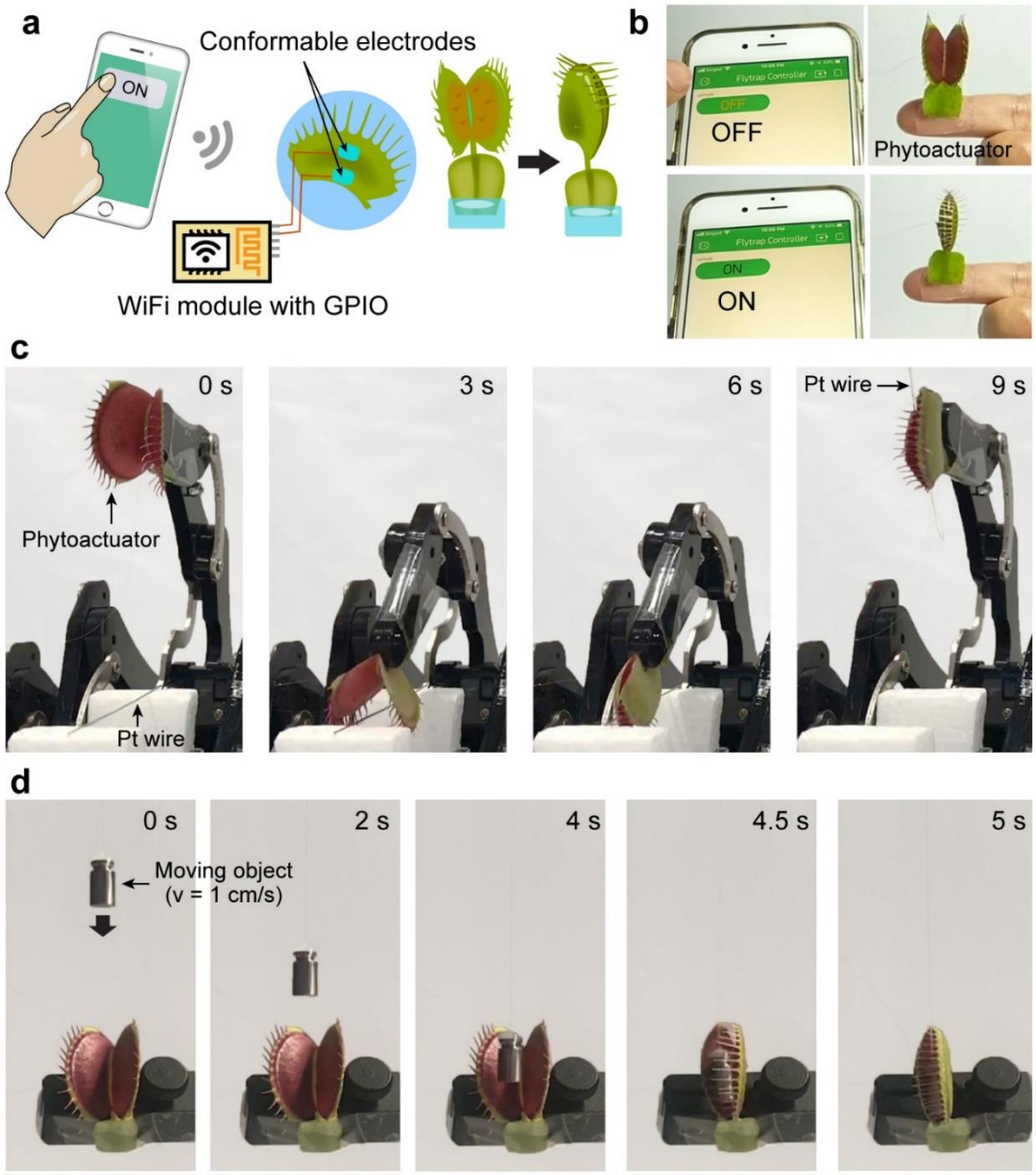

Fig. 4 | Integration of modular electrical phytoactuator with other platforms. a, Schematic showing the implementation of the smartphone-controllable phytoactuator. An "ON" command from the smartphone application is sent via the Internet to a WiFi module (ESP8266) with General Purpose Input Output (GPIO). The WiFi module then sends a 3.3 V square wave to the conformable electrodes, which triggers the flytrap closure. b, Photograph of the phytoactuator as controlled by a smartphone. c, Photos showing the integration of the phytoactuator with a robotic hand enables the hand to perform delicate tasks such as grasping a thin (0.5 mm diameter) Pt wire. d, Photos showing accurate modulation of the flytrap

response time allows the phytoactuator mounted on a manipulator to capture a moving object (1 g weight) at a velocity of 1 cm/s.

Methods

Fabrication of conformable electrodes. The Au nanomesh film was synthesized as previously reported[36, 37]. Briefly, 4.8 mg of Gold (III) chloride trihydrate ($HAuCl_4 \cdot 3H_2O$, Sigma-Aldrich) was dissolved in 25 mL DI water. The $HAuCl_4$ solution was poured in a 250 mL glass beaker and subjected to 400 rpm stirring at 5 °C. Subsequently, 1.2 mg of Sodium borohydride ($NaBH_4$, Fluka Analytical) was dissolved in 25 mL DI water as reduction agent. The $NaBH_4$ solution was slowly added to the $HAuCl_4$ solution drop by drop, while the bath temperature was kept at 5 °C and stirring rate kept at 400 rpm. As $NaBH_4$ was added, the solution changed to red wine color. After adding $NaBH_4$, 100 mL toluene (VWR Chemicals) was added to the mixed solution and the solution was kept at 5 °C and 600 rpm for 15 min. Then the solution was rested in ambient condition for another 30 min. There would be obvious layer separation with toluene at the top layer and dark reddish aqueous solution at the bottom layer. Toluene was removed and after thorough evaporation of toluene residuals, there was an Au nanomesh film formed on the top of the water surface. PDMS film was prepared by mixing SYLGARD 184 silicone elastomer base and curing agent at a ratio of 10:1, spin-coated on a Si wafer at 800 rpm for 60s and cured at 80 °C for 5 h. PDMS film was first attached to a PET (polyethylene terephthalate) film and the PET-PDMS film was cut into the desired shape for Au nanomesh transfer. The PET-PDMS film was put in contact with the Au nanomesh on top of the water surface, the contact was kept for 20 s for a complete transfer. Then the PET-PDMS-Au nanomesh film was lifted and allowed to dry at ambient condition. PDMS film was peeled off from PET for further usage. To fabricate soft hydrogel-Au nanomesh-PDMS electrode, PAA (polyacrylic acid) hydrogel precursor solution was first prepared. Briefly, in 4 mL DI water, 1 mL acrylic acid (Sigma-Aldrich), 20 mg potassium chloride (Sigma-Aldrich), 40 mg potassium persulfate (Sigma-Aldrich), 1.67 mg N,N'-Methylenebisacrylamide (Sigma-Aldrich), 40 μL N,N,N',N'-Tetramethylethylenediamine (Sigma-Aldrich), were subsequently added. To make PAA

hydrogel in the desired shape, a handmade PDMS mold was made first. The PDMS mold with 3 mm × 3 mm wells was put on top of the glass substrate and PAA hydrogel precursor solution was poured into the PDMS wells. The PDMS mold was covered by a petri dish and heated in an oven at 70 °C for 15 min. After the heating process, the hydrogel formed in the PDMS mold and was washed with 0.1M KCl aqueous solution for 30 min. The washed hydrogel was transferred onto PDMS-Au nanomesh film, forming PDMS-Au nanomesh-hydrogel electrode. One end of the electrode was wired by a copper wire dipped in a liquid metal point (Gallium–Indium eutectic, Sigma-Aldrich). Ecoflex elastomer was used to seal the wiring point.

Characterization of synthesized Au nanomesh. As-synthesized Au nanomesh on the water surface was lifted by the Cu grid and allowed to thoroughly dry, the Au nanomesh sample on the Cu grid was observed by field emission transmission electron microscopy (TEM, JEOL, JEM-2100F) for nanostructure and morphology studies. Au nanomesh aqueous solution was collected and light absorption was analysed using UV-vis spectroscopy (SHIMADZU UV-2550 UV-vis spectrophotometer). Au nanomesh transferred on PDMS was characterized by field emission scanning electron microscopy (SEM, JEOL, 7600F). The Au nanomesh-PDMS film was also characterized by UV-vis spectroscopy (SHIMADZU UV-2550 UV-vis spectrophotometer) for transmittance studies.

Electrical characterization of the conformable electrodes. The cyclability of the Au nanomesh-PDMS film (3 cm x 1 cm) was measured by a parameter analyzer (Keithley 4200) and a mechanical tester (MTS Criterion Model C42). A 50% strain was applied to the film at a strain rate of 0.2 mm/s for 200 times by the mechanical tester. The resistance of the film was recorded by the parameter analyzer. The stretchability of the Au nanomesh-PDMS film (3 cm × 1 cm) was measured by a parameter analyzer (Keithley 4200) and a mechanical tester (MTS Criterion Model C42). The film was stretched at a strain rate of 0.2 mm/s until rupture. The resistance of the film was recorded by the parameter analyzer. The interfacial impedance

between electronic films and hydrogel was measured by an electrochemical workstation (Zennium E, Zahner Ennium). A hydrogel film (1 cm × 1 cm) was sandwiched by two Au nanomesh-PDMS films (2 cm × 1 cm), with Au nanomesh in contact with two sides of the hydrogel film. The impedance of Au nanomesh-hydrogel-Au nanomesh was measured from 1 Hz to 10^6 Hz. Admittance was calculated as reciprocal of impedance to reflect the ease of current transduction from Au nanomesh to the hydrogel. As control groups, AgNW and CNT on PDMS film (2 cm × 1 cm) with the similar conductance as that of Au nanomesh film, and Ai foil were also measured with the same sandwich configuration. AgNW and CNT films were prepared by vacuum filtration method, where AgNW and CNT were first filtrated on a filter paper, and then transfer-printed on a PDMS film, the conductance of AgNW and CNT films were tuned by the amount of solutions filtrated on the filter paper.

Adhesive strength of hydrogel on the plant leaf surface. The adhesive strength of hydrogel on the plant leaf surface was evaluated by a 90° peel-off experiment. Briefly, the hydrogel film was synthesized with a pre-defined dimension of 40 mm × 15 mm × 0.1 mm on a polyimide film. Polyimide film was used as a backing layer to restrict the elongation of the hydrogel during peeling, thus the force applied is mostly used for peeling rather than straining. On the mechanical tester (MTS Criterion Model C42), a leaf was cut into a rectangular shape and was fixed on the bottom plate of the mechanical tester with double tape. Hydrogel with polyimide backing was pressed onto the leaf surface and one end was fixed with upper gripper. The strain rate was set at 0.2 mm/s and the hydrogel with polyimide backing was slowly peeled off from the leaf. The plateau of force during pealing was averaged and divided by hydrogel width as adhesive strength.

Chlorophyll content measurement of leaf after applying adhesive hydrogel. The chlorophyll content of the plant after applying hydrogel was evaluated with a chlorophyll meter (SPAD 502 Chlorophyll Meter) on Devil's ivy (*Epipremnum aureum*). Devil's ivy was selected as a model plant in chlorophyll measurement, as it has large and mechanical-

insensitive leaves for chlorophyll meter clipping, while its leaf texture and thickness are similar to Venus flytrap. Briefly, a hydrogel film (0.5 cm × 0.5 cm) with PDMS cover was attached on the leaf of Devil's ivy, the chlorophyll content was measured every 1 hour for 10 hours. 6 leaves were examined with the chlorophyll meter.

On-plant impedance measurement. The impedance between two conformable electrodes on the plant surface was measured as on-plant impedance. Aloe vera was used as a model plant to test on-plant impedance. Flytrap usually presents thin and irregular petioles, making it difficult to directly measure on-plant impedance with a standardized protocol. On the other hand, Aloe vera shows large surfaces, different electrodes can be applied to it with the same measurement protocols. Briefly, the surface of one Aloe vera stem was cleaned with Kimwipe, then conformable electrodes with a pre-defined area of 1 cm × 1 cm were attached to the Aloe vera surface separated by 1 cm. The impedance between the two electrodes was measured by an electrochemical workstation (Zennium E, Zahner Ennium) at a frequency range from 1 Hz to 10^6 Hz. After the measurement of conformable electrodes, the electrodes were peeled off and cleaned with Kimwipe again, Ag/AgCl-Agar electrodes were placed in the same position. The same settings were used for the Ag/AgCl-Agar on-plant impedance measurement.

Mechanical stimulation of flytrap. Flytraps were purchased from ANR Technologies in Singapore. All the flytraps were grown from tissue culture. Two conformable electrodes (3 mm × 3 mm) were attached to flytrap in a pot. One conformable electrode was attached to the center of the lower epidermis of flytrap as a recording electrode (positive terminal), the other conformable electrode was attached on the petiole surface of flytrap as a reference electrode (negative terminal). One mechanosensitive hair of flytrap was gently hovered by a woody stick. The mechanosensitive hair was stimulated every 100 s, this can confirm a generation of a series AP every 100 s but not close the flytrap lobes. Electrical signals measurement was conducted in a home-made Faraday cage. The two terminals were connected to the analog

inputs of a data acquisition system (USB-2610 Series DAQ, Smacq Technologies) in the Faraday cage without using a low-pass filter. There are no observable high-frequency noises in the measured signals. The data acquisition system was operated in differential mode to reject common-mode noises and was sampled at 100 Hz sampling rate. The sampling rate was verified as shown in Supplementary Fig. 15. The ground terminal of the data acquisition system was connected with the Faraday cage for shielding of EMI (electromagnetic interference).

Electrical stimulation of flytrap. Four conformable electrodes (two pairs, 3 mm × 3 mm each) were attached to two lower epidermis of the flytrap lobe (Fig. 2a). For the applied voltage pair, the positive terminal was attached near the midrib and the negative terminal was attached to the center of the lobe. For the potential signal measurement pair, the positive terminal was attached to the center of the lobe and the negative terminal was attached near the midrib. For DC stimulation, the applied voltage pair was connected to a Keithley Source Meter (Keithley 2450). The current was simultaneously measured using the Keithley Source Meter during applying voltage stimulation. For frequency-dependent stimulation, the applied voltage pair was connected to a function generator (Keysight Technologies 33210A). 3 V square waves at different frequencies (0.1 Hz, 0.25 Hz, 0.5 Hz, 1 Hz, and 2 Hz) were supplied by the function generator. The electrical signal measurement pair was connected to analog inputs of a data acquisition system (USB-2610 Series DAQ, Smacq Technologies) using differential mode at a 100 Hz sampling rate. All the measurements were conducted in a Faraday cage.

Data processing and analysis. The normalized flytrap lobe edge distance (y/y_0) was used to reflect the flytrap lobe closing process. A camera was placed in front of the flytrap under study to take a video of the flytrap closing. The video was converted to a series of images at a sampling rate of 10 frames/sec. The changing flytrap lobe edge distance (y) was measured using ImageJ, and all the y values were divided by the initial lobe edge distance

before flytrap closing (y_0). The y/y_0 data were aligned with applied voltage data or potential signal data in time sequence to study the relationships between electrical stimulation, action potential, and flytrap actuation. The response time was extracted from y/y_0 data by annotating the time of the start of electrical stimulation and the start of the flytrap closing. This time interval was noted as response time. The first two-AP interval was extracted from potential signal data. The time points where the first AP peak maxima appeared, and second AP peak maxima appeared were annotated and subtracted. This time interval was noted as the first two-AP interval. The correlation of the response time and the first two-AP interval was fitted by a line without fixing intercept or slope. The AP interval was analyzed based on the series AP data of potential signals under DC stimulation. The time points where AP maxima appeared were annotated, and neighboring time points were subtracted to get time intervals. The time intervals are noted as AP intervals. The normalized actuating speed of modular flytrap from DC stimulation and 2 Hz stimulation were obtained by taking the first-order derivative of y/y_0 data (Supplementary Fig. 28) and the data points are connected with B-spline.

Fabrication of electrically modulated phytoactuator. The electrically modulated phytoactuator was made by flytrap and conformable electrodes. The phytoactuator was worn on a finger and controlled by a smartphone, integrated with a robotic arm to pick up a fine wire, and integrated on a manipulator to capture moving objects. Flytrap was cut from its petiole and the cutting area was immediately sealed with Ecoflex elastomer. Two conformable electrodes (3 mm × 3 mm) were attached to the lower epidermis of one flytrap lobe. The positive terminal was attached near the midrib and the negative terminal is attached to the center of the lobe. The two conformable electrodes were connected with two GPIO (General Purpose Input Output) terminals of the WiFi module (ESP8266). The positive terminal was connected to an OUTPUT terminal of the WiFi module, the negative terminal was connected to a GND (ground) terminal of the WiFi module. The WiFi module was programmed to

communicate with a smartphone by a customized mobile app using the Blynk IoT platform. The codes to program the WiFi module ESP8266 can be found in Github (https://github.com/Wenlong0-0/Wireless-control-of-phytoactuator). A D-Link router was used to allow internet access to the WiFi module. The programmable bionic robotic hand (μhand) was purchased from VANBOT. The moving object was controlled by a customized LabVIEW motorized device.

References

1. Rus, D. & Tolley, M.T. Design, fabrication and control of soft robots. *Nature* 521, 467 (2015).
2. Walsh, C. Human-in-the-loop development of soft wearable robots. *Nat. Rev. Mater.* 3, 78-80 (2018).
3. Rich, S.I., Wood, R.J. & Majidi, C. Untethered soft robotics. *Nat. Electron.* 1, 102-112 (2018).
4. McEvoy, M.A. & Correll, N. Materials that couple sensing, actuation, computation, and communication. *Science* 347, 1261689 (2015).
5. Kim, Y., Parada, G.A., Liu, S. & Zhao, X. Ferromagnetic soft continuum robots. *Sci. Robot.* 4, eaax7329 (2019).
6. Li, S., Vogt, D.M., Rus, D. & Wood, R.J. Fluid-driven origami-inspired artificial muscles. *Proc. Natl. Acad. Sci.* 114, 13132-13137 (2017).
7. Yang, H. *et al.* 3D Printed Photoresponsive Devices Based on Shape Memory Composites. *Adv. Mater.* 29, 1701627 (2017).
8. Vatankhah-Varnoosfaderani, M. *et al.* Bottlebrush Elastomers: A New Platform for Freestanding Electroactuation. *Adv. Mater.* 29, 1604209 (2017).
9. Morimoto, Y., Onoe, H. & Takeuchi, S. Biohybrid robot powered by an antagonistic pair of skeletal muscle tissues. *Sci. Robot.* 3, eaat4440 (2018).
10. Li, Z. *et al.* Biohybrid valveless pump-bot powered by engineered skeletal muscle. *Proc. Natl. Acad. Sci.* 116, 1543-1548 (2019).
11. Ricotti, L. *et al.* Biohybrid actuators for robotics: A review of devices actuated by living cells. *Sci. Robot.* 2, eaaq0495 (2017).
12. Cai, P. *et al.* Biomechano-Interactive Materials and Interfaces. *Adv. Mater.* 30, 1800572 (2018).
13. Feinberg, A.W. *et al.* Muscular Thin Films for Building Actuators and Powering Devices. *Science* 317, 1366-1370 (2007).
14. Appiah, C. *et al.* Living Materials Herald a New Era in Soft Robotics. *Adv. Mater.* 31, 1807747 (2019).
15. Trewavas, A. Plant intelligence: Mindless mastery. *Nature* 415, 841 (2002).
16. Mousavi, S.A.R., Chauvin, A., Pascaud, F., Kellenberger, S. & Farmer, E.E. GLUTAMATE RECEPTOR-LIKE genes mediate leaf-to-leaf wound signalling. *Nature* 500, 422 (2013).
17. TREWAVAS, A. What is plant behaviour?*. *Plant Cell Environ.* 32, 606-616 (2009).
18. Skrzypczak, T. *et al.* Plant Science View on Biohybrid Development. *Front. Bioeng. Biotechnol.* 5 (2017).
19. F. Baluska, M.G., G. Witzany *Memory and Learning in Plants*. (Springer, Switzerland; 2018).
20. Boudaoud, A. An introduction to the mechanics of morphogenesis for plant biologists. *Trends Plant Sci.* 15, 353-360 (2010).
21. Qi, J. *et al.* Mechanical regulation of organ asymmetry in leaves. *Nat. Plants* 3, 724-733 (2017).
22. Chen, H. *et al.* Ultrafast water harvesting and transport in hierarchical microchannels. *Nat. Mater.* 17, 935-942 (2018).
23. Barthlott, W., Mail, M., Bhushan, B. & Koch, K. Plant Surfaces: Structures and Functions for Biomimetic Innovations. *Nano-Micro Lett.* 9, 23 (2017).
24. Markin, V.S., Volkov, A.G. & Jovanov, E. Active movements in plants. *Plant Signal Behav.* 3, 778-783 (2008).

25. Scherzer, S., Federle, W., Al-Rasheid, K.A.S. & Hedrich, R. Venus flytrap trigger hairs are micronewton mechano-sensors that can detect small insect prey. *Nat. Plants* 5, 670-675 (2019).
26. Hedrich, R. & Neher, E. Venus Flytrap: How an Excitable, Carnivorous Plant Works. *Trends Plant Sci.* 23, 220-234 (2018).
27. Volkov, A.G., Adesina, T. & Jovanov, E. Closing of venus flytrap by electrical stimulation of motor cells. *Plant Signal Behav.* 2, 139-145 (2007).
28. Volkov, A.G., Adesina, T. & Jovanov, E. Charge induced closing of Dionaea muscipula Ellis trap. *Bioelectrochemistry* 74, 16-21 (2008).
29. Grimnes, S. & Martinsen, Ø.G. Electrodes, in *Bioimpedance and Bioelectricity Basics (Third Edition)*. (eds. S. Grimnes & Ø.G. Martinsen) 179-254 (Academic Press, Oxford; 2015).
30. Volkov, A. *Plant Electrophysiology Theory and Methods*. (Springer, 2006).
31. Salvador-Recatalà, V., Tjallingii, W.F. & Farmer, E.E. Real-time, in vivo intracellular recordings of caterpillar-induced depolarization waves in sieve elements using aphid electrodes. *New Phytol.* 203, 674-684 (2014).
32. Reedus, J. *et al.* Memory elements in the electrical network of Mimosa pudica L. AU - Volkov, Alexander G. *Plant Signal Behav.* 9, e982029 (2014).
33. Mousavi, S.A.R., Nguyen, C.T., Farmer, E.E. & Kellenberger, S. Measuring surface potential changes on leaves. *Nat. Protoc.* 9, 1997 (2014).
34. Kim, J.J., Allison, L.K. & Andrew, T.L. Vapor-printed polymer electrodes for long-term, on-demand health monitoring. *Sci. Adv.* 5, eaaw0463 (2019).
35. Naficy, S., Razal, J.M., Whitten, P.G., Wallace, G.G. & Spinks, G.M. A pH-sensitive, strong double-network hydrogel: Poly(ethylene glycol) methyl ether methacrylates–poly(acrylic acid). *J. Polym. Sci., Part B: Polym. Phys.* 50, 423-430 (2012).
36. Ramanath, G. *et al.* Templateless Room-Temperature Assembly of Nanowire Networks from Nanoparticles. *Langmuir* 20, 5583-5587 (2004).
37. Ho, M.D., Liu, Y., Dong, D., Zhao, Y. & Cheng, W. Fractal Gold Nanoframework for Highly Stretchable Transparent Strain-Insensitive Conductors. *Nano Lett.* 18, 3593-3599 (2018).
38. Trebacz, K. & Sievers, A. Action Potentials Evoked by Light in Traps of Dionaea muscipula Ellis. *Plant and Cell Physiology* 39, 369-372 (1998).
39. Volkov, A.G., Adesina, T., Markin, V.S. & Jovanov, E. Kinetics and Mechanism of Dionaea muscipula Trap Closing. *Plant Physiol.* 146, 694-702 (2008).
40. Miyamoto, A. *et al.* Inflammation-free, gas-permeable, lightweight, stretchable on-skin electronics with nanomeshes. *Nat. Nanotechnol.* 12, 907 (2017).
41. Yuk, H., Lu, B. & Zhao, X. Hydrogel bioelectronics. *Chem. Soc. Rev.* 48, 1642-1667 (2019).
42. Liu, Y. *et al.* Soft and elastic hydrogel-based microelectronics for localized low-voltage neuromodulation. *Nat. Biomed. Eng.* 3, 58-68 (2019).
43. Stavrinidou, E. *et al.* Electronic plants. *Sci. Adv.* 1, e1501136 (2015).
44. Wong, M.H. *et al.* Nitroaromatic detection and infrared communication from wild-type plants using plant nanobionics. *Nat. Mater.* 16, 264 (2016).
45. Stavrinidou, E. *et al.* In vivo polymerization and manufacturing of wires and supercapacitors in plants. *Proc. Natl. Acad. Sci.* 114, 2807-2812 (2017).

Acknowledgments

The authors acknowledge financial support from the National Research Foundation (NRF), Prime Minister's Office, Singapore, under its NRF Investigatorship (NRF2016NRF-NRF1001-21) and the Agency for Science, Technology and Research (A*STAR) under its AME Programmatic Funding Scheme (project no. A18A1b0045) Cyber-Physiochemical Interfaces (CPI) Programme. N. M. was supported by Japan Society for the Promotion of Science (JSPS) overseas research fellowship. Finally, the authors thank Dr. Ai Lin Chun for critically reading and editing the manuscript.

Author contributions

W. L., N. M., and X. C. designed the project and experiments. Z. Y. L. assisted with conformable electrode design, fabrication, and characterization. W. L. and M. W. synthesized and characterized the adhesive hydrogel. Y. L. and W. L. performed an optical cross-section microscope of plant and hydrogel. P. C. assisted with conformable electrode fabrication. G. C. and W. L. designed and performed adhesive strength measurement of the electrode. W. L., F. Z., and C. L. performed flytrap electrical signal measurement, flytrap mechanical and electrical stimulation, and phytoactuator implementation. Z. H. L. designed and manufactured the LabVIEW-controlled motorized device for accurate capture of moving objects. Z. S. L. and W. L. fabricated AgNW and CNT conductors. W. Z. performed TEM investigation for Au nanomesh. W. L., N. M., and X. C. wrote the manuscript. All authors read and revised the manuscript.

Competing interests

The authors declare no competing interests.

Additional information